Hot Straining and Quenching and Partitioning of a TRIP-assisted Steel: Microstructural Characterization and Mechanical Properties

Edwan Anderson Ariza[1,3a*], Jonathan Poplawsky[2,b], Wei Guo[2,c], André Paulo Tschiptschin[1,d*]

[1]Department of Metallurgical and Materials Engineering, University of São Paulo, Av. Prof. Mello Moraes, 2463 – Cidade Universitária, Butantã, São Paulo-SP. Brazil.

[2]Materials Science and Technology Division, Oak Ridge National Laboratory, P.O. Box 2008, Oak Ridge-TN 37831-6139, USA

[3]Mechanical Technology Program. Technological University of Pereira, Pereira. Colombia

[a]andersonariza@usp.br, [b]poplawskyjd@ornl.gov, [c]guow1@ornl.gov, [d]antschip@usp.br

Keywords: TRIP-steel, 3rd Generation Advanced High-Strength Steel, Carbon Partitioning

Abstract. Advanced high strength steels (AHSS), with yield strengths and tensile strengths above 400 and 700 MPa, respectively, are becoming more noticeable in vehicle manufacturing. A novel processing route of a TRIP-assisted steel was developed. Characterization and modelling techniques were used to establish correlations between processing, microstructure and mechanical properties. TRIP-assisted steel was heat-treated by quenching and partitioning (Q&P) and a novel process of hot straining (HS) and Q&P (HSQ&P) treatments on a Gleeble ®3S50 thermo-mechanical simulator. The samples were intercritical annealed at 800 ºC, quenched at 318 ºC (optimal quenching temperature), and partitioned at 400 ºC for 100 s. In the HSQ&P process, isothermal straining at 800 ºC was applied. The influence of isothermal straining at high temperatures on the strain-induced transformation to ferrite (SIT) effect, austenite carbon enrichment, and carbide precipitation were investigated. Carbon, silicon, and manganese distribution in the martensite/austenite interfaces and carbide formation were analyzed by means of atom probe tomography (APT). The carbon enrichment in austenite was confirmed in all samples. The carbon enrichment in Q&P samples was slightly inferior than in HSQ&P, suggesting the contribution of the additional carbon partitioning to austenite from ferrite formed by the SIT-effect. The carbon accumulation at the interface of martensite/austenite was clearly observed by APT. The newly developed combined thermomechanical process (HSQ&P) is promising as the transformation induced plasticity can favor the energy absorption and formability, contributing to fill the gap of the third generation of high-strength steels.

Introduction

Untransformed austenite at room temperature can transform into martensite through plastic deformation, improving the ductility and mechanical properties through the transformation induced plasticity (TRIP) phenomenon. It is well documented that high carbon concentration of austenite decreases the martensite start temperature (Ms), causing the austenite stabilizing [1,2]. Recently, quenching and partitioning (Q&P) heat treatment [3] is currently being studied more in depth because of the formation of carbon-enrichment austenite due to carbon partitioning from martensite into remained austenite at partitioning stage. Therefore, this heat treatment has been widely employed in automotive industries where both high strength and elongation are required.

Three-dimensional nanoscale characterization method analyzed by Atom Probe Tomography (APT) allows us to observe the distribution of carbon and specific chemical elements. Although, Toji et al. [4] and Clarke et al. [5] employed this technique to characterize and quantify the distribution and preferred sites of carbon in Q&P specimens, very few studies [6–9] have been performed to evaluate the carbon distribution under deformation at hot temperatures followed by Q&P treatment. Hence, the microcharacterization by APT allows clarification as to whether the SIT

effect [10] favors austenite carbon enrichment and/or whether during ferrite precipitation there were also carbides precipitation making difficult the carbon diffusion to neighboring austenite.

In the current study, TRIP-assisted steel was annealed at intercritical temperature then subjected to hot straining followed by a two-step Q&P treatment (called as HSQ&P). Then, the redistribution of carbon was studied using APT in both Q&P and HSQ&P samples to investigate the effect of hot straining on the development of complex microstructures and the resultant mechanical properties of AHSS.

Experimental Procedure

Commercial TRIP-assisted steel containing 0.23C–1.23Si–1.50Mn, wt.% was studied in this research. Thermomechanical heat treatments (i.e., Q&P and HSQ&P) were carried out using a Gleeble®3S50 thermomechanical simulator. As-received TRIP steel was fully austenitized at 1000 °C for 5 min to homogenization and remove residual stress and history of previous mechanical treatment on microstructure. Then, the specimens were rapidly cooled down in the intercritical region at 800 °C and maintained for 5 min. For the HSQ&P process, samples were hot strained at the intercritical temperature specimens in 30% (true strain) and the initial straining temperatures were 800 °C. According to the Koistinen and Marburger equation, the optimum quenching temperature to obtain the maximum retained austenite fraction at room temperature was determined to be 318 °C. The specimens were rapidly quenched (at 60 °C/s) to 318 °C (Q_T) for 5 s. Then, the samples, for the partitioning stage, were reheated to 400 °C (at 15 °C/s) for 100 s.

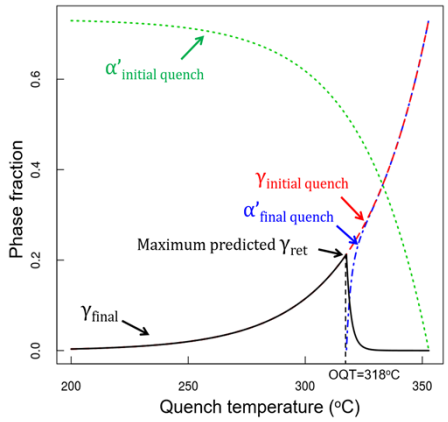

Fig. 1: Calculation of optimum quenching temperature (OQT) for achieving the maximum volume fraction of retained austenite in the final microstructure of the investigated steel. $\alpha'_{\text{initial quench}}$ and $\gamma_{\text{initial quench}}$ are the initial martensite and austenite fractions at quenching temperature, and $\alpha'_{\text{final quench}}$ and γ_{final} are the final austenite and martensite fractions of martensite and austenite at room temperature.

For microscopic analysis by optical and scanning electron microscopy (SEM) specimens were prepared by standard metallographic procedures and etched using 2% Nital. Using a FEI-Inspect 50 field emission gun scanning electron microscope (FEG-SEM), microstructural analyses were carried out.

For APT measurements, regions previously identified by EBSD as austenite and martensite interfaces were extracted using focused ion beam (FIB). The samples were annularly milled with an acceleration voltage of 30 kV and cleaned with a 5 kV for a proper field evaporation. The experiments were conducted using a CAMECA Instruments LEAP® 4000X HR local electrode atom probe, with improved mass resolution from using an energy-compensating reflectron lens. In laser mode, the samples were field evaporated with a 200 kHz pulse repetition rate at 30 °C, with a laser power of 50 pJ, and a detection rate of 0.5–1.0%. The data were analyzed using the CAMECA IVAS software®. Based on the natural abundances of the chemical elements, the ions deconvolution within overlapping isobars of different elements (e.g., Cr54/Fe54 and $C2^{+}/C4^{++}$) was performed.

Uniaxial tensile tests were conducted at room temperature using an Instron model 3369 servo-hydraulic testing machine at a strain rate of 1.0×10^{-3} s^{-1}.

Results and Discussion

Microstructural Characterization.

The microstructure of Q&P and HSQ&P specimens were studied using optical microscopy (OM) and scanning electron microscopy (SEM), as presented in Figure 2. Multi-phase microstructure containing ferrite (α), martensite (α'), and retained austenite (γ) was observed in both samples. By light OM (Figs. 2a-b), the α is revealed as white and by SEM appears dark (Figs. 2a and 2c). The α' plates (enclosing films of γ) are revealed as dark brown in the optical micrographs or light gray by SEM. In Fig. 2b, it is possible to observe that straining the γ prior to the Q&P heat treatment influences the final microstructure, revealing refinement of the α' packet and block sizes. The volume fraction of α phase was measured from the OM micrographs through linear intercept method. A 15% increment of the volumetric fraction of the ferritic phase was found when applying hot straining. This increase could be explained by strain-induced transformation to ferrite (SITF) mechanism due to the acceleration of the nucleation rates and α growth after the intercritical straining, which can cause a higher C content available to diffuse in γ. Thus, carbon enrichment in γ with high stability could be obtained.

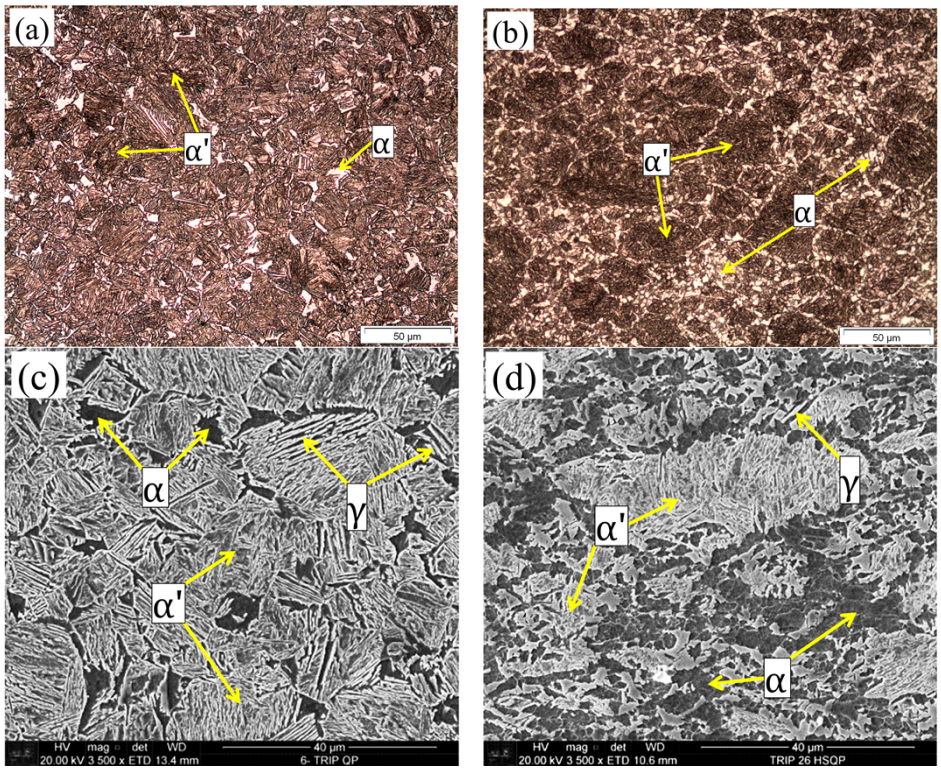

Fig. 2: Microstructures of the investigated steel. (a,c) Q&P and (b,d) HSQ&P.

APT - Q&P.

Figure 3a shows the FIB-deposited Pt rectangle covering the region of interest (ROI) for analysis (martensite/austenite interface) and nanoindentation marks. Carbon content distribution inside the cylinders, as seen in Figure 3b, was calculated as 0.23 at.%, 5.5 at.%, and 25 at.% in the α', γ, and cementite (θ or Fe3C) regions, respectively. The atomic fractions of C, Mn, and Si using proximity histograms were estimated by means of isoconcentration surfaces at 2 at.%. The distribution of C, Si, and Mn at martensite/retained austenite interphase was demonstrated in Figure 3c. No variation was observed for Si and Mn substitutional elements. However, the significant carbon partitioning was found at α'/γ interphase. This finding can prove the development of low-carbon low tetragonal body-centered cube (BCC) martensite at the vicinity of retained austenite. The distribution of C and Si atoms at the martensite/θ precipitate interface was also shown in Figure 3d. According to the CCE criterion, all C migrates from martensite to austenite during partitioning stage. Therefore, a remarkable deviation of this model could be considered due to the effect of carbide formation during Si migration, leading to a reduction of the potential for the C enrichment of γ. However, the presence of θ in the α', evidenced in the APT measurements, clearly indicates that the suppression

of carbide precipitation considered in the CCE model does not comply, even for steels containing Si (1.23 wt.%). Si can retard carbide formation, leading to an increase of the carbon partitioning into remaining austenite, favoring its high stability and enhancing the toughness of the material. Figure 3c also exhibited the carbon accumulation at the α'/γ interface, where carbon concentration reached approximately 7.6 at.%, indicating a negative C gradient in the γ. Hence, APT technique provides strong evidence for carbon partitioning from α' to γ. Here lies the different between the carbon solubilities, supersaturated ferrite (α') and austenite (γ). In the partitioning step, the system seeks to balance the chemical potential of C, giving rise to a C diffusive flux from α' to γ.

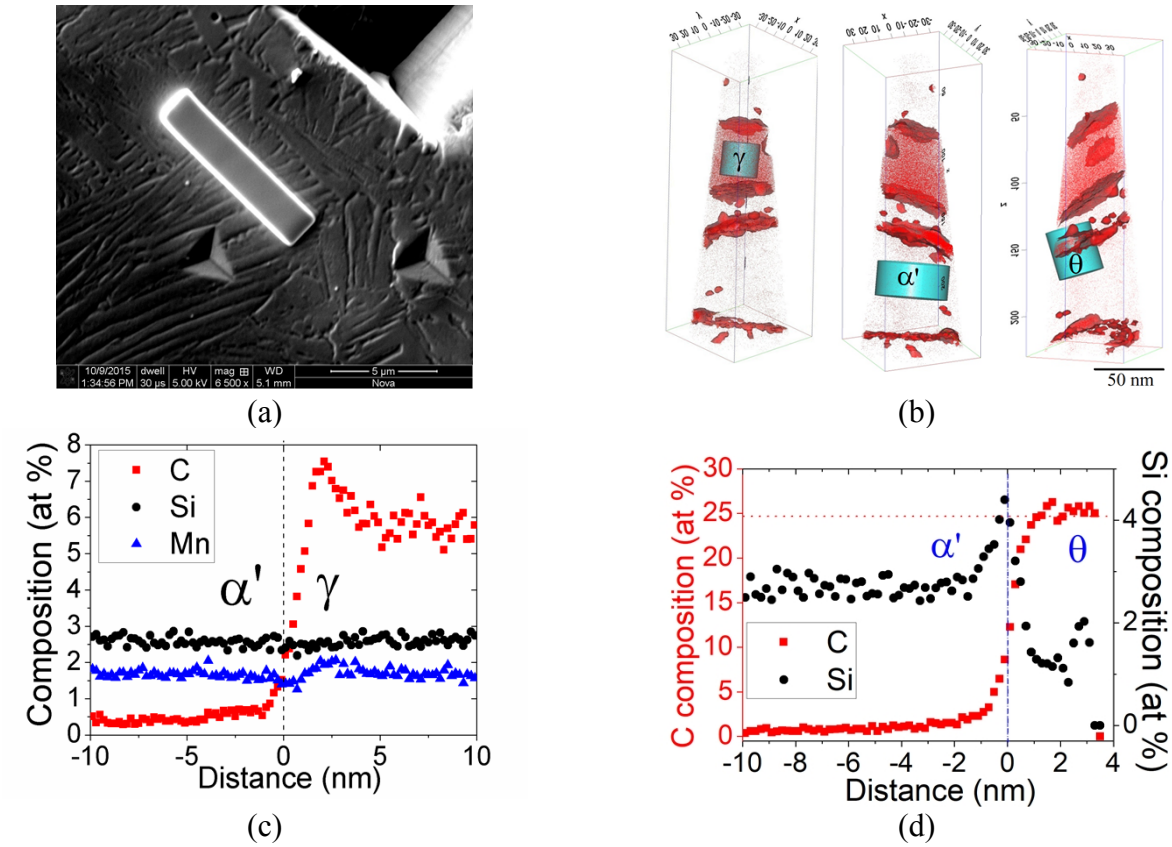

Fig. 3: (a) FIB-deposited Pt covering the ROI, (b) C isoconcentration surfaces at 2 at%, superimposed with the C atom map. Also observed in this figure are the cylinders for the chemical composition analysis, (c,d) proximity histograms obtained across the martensite (α')/austenite (γ) interface and through a cementite (θ or Fe_3C)/α' interface.

APT-HSQ&P.

Figure 4 shows the APT results of the HSQ&P sample. To measure the carbon content in the γ and α', a cylinder of ≈ 50 nm diameter and a sphere of ≈ 30 nm diameter respectively were placed on these regions, as shown in Fig. 4a. The atomic percentage of carbon was quantified as 0.11 at.% within the marked sphere, while enriched retained austenite contains about 6-7 at.%. The formation of α_{SITF} accelerates the carbon partitioning during hot straining and contributes to the formation of carbon enrichment austenite. No variation of the distribution of Si and Mn elements were found at α'/γ interface at 400 °C, which is consistent with Q&P samples. Carbide precipitation was also characterized in the analyzed cylinder. The carbon content at this precipitate was calculated at about 23 at.% which is very close to the stoichiometric C concentration in cementite (25 at.% C). Due to the high driving force for precipitation of carbides from the C supersaturated α', carbide precipitation is basically unavoidable. Hence, the partitioning of C from α' → γ and the tempering process occur simultaneously, however they are not mutually exclusive in the thermomechanical processes conducted. Consequently, one of the main considerations of the CCE model – the absence of Fe_3C formation during the partitioning stage – is not met. One of the main conclusions of these results is the strong evidence of the development of high carbon-enrichment in the remained

austenite in the HSQ&P samples. High carbon concentration in austenite increases its stability at room temperature, improving significantly the toughness and limiting the premature failure. In addition, in HSQ&P samples the C partitioning into γ from supersaturated α', intercritical α, and α induced by deformation are essential for γ stabilization. The knowledge of these effects is essential for the understanding of the phase composition and morphology of the final microstructure and, therefore, the final mechanical properties of the material.

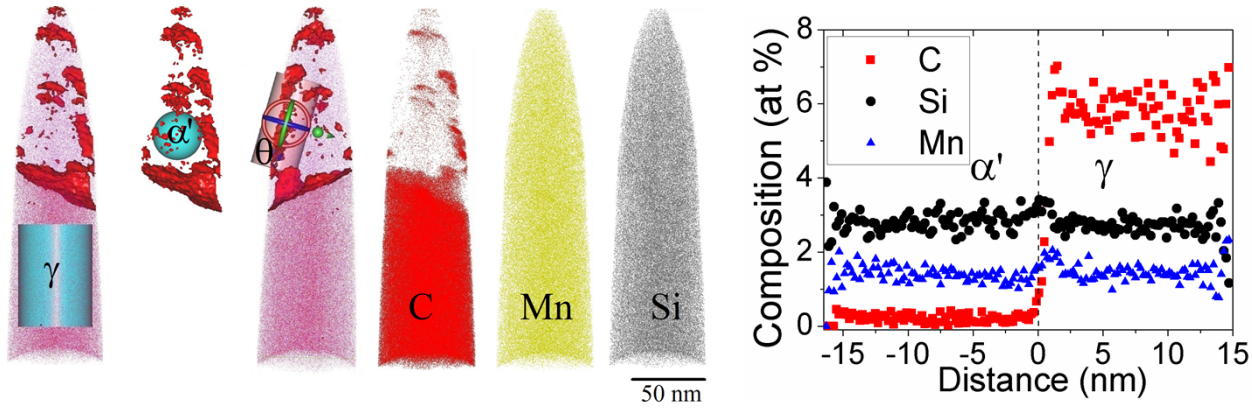

(a) (b)

Fig. 4: (a) C isoconcentration surfaces at 3 at.% C and 3-D elemental atom maps of C, Mn, and Si, and (b) proximity histograms across α'/γ interface.

Mechanical Properties.

Uniaxial tensile test was conducted for both Q&P and HSQ&P samples and the resulting stress-strain curves are presented in Figure 5. It can be seen that the Q&P sample has higher yield stress (≈ 978 MPa) and ultimate tensile strength (≈ 1035 MPa) than HSQ&P specimen (≈ 820 and ≈ 920 MPa). However, the total elongation of the HSQ&P (≈ 23%) is higher than the Q&P (≈ 15%). The lower tensile strength accompanied with higher elongation is related to the formation of a high fraction of stable carbon enrichment austenite, which through TRIP effect enhances the toughness of HSQ&P sample. In addition, excess carbon partitioning during hot straining led to carbon depletion in martensite (carbon content in α'; Q&P ≈ 0.23 at.%C and HSQ&P ≈ 0.11 at.%C). Thus, low-tetragonal martensite was developed in HSQ&P processing, which can enhance strain hardening performance and avoids premature failure. Absorbed energy behavior was calculated from the area below tensile engineering stress-strain curves. This value in the HSQ&P sample was higher (21.2 MPa%) than in the Q&P (15.5 MPa%) sample, demonstrating its better mechanical performance. Hence, the HSQ&P specimens would allow the manufacture of high strength components with good plasticity, and the decrease of vehicle weight with the option of fabricating plates thickness much thinner and lighter. Additionally, the greater austenite stabilization is preferred in the applications of steels of the automotive industry because it will favor the TRIP-effect during impact, increasing the safety of the passengers through energy absorption [7].

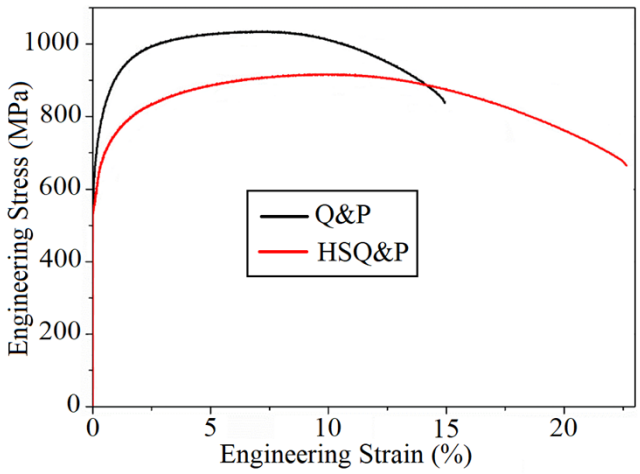

Fig. 5: Tensile engineering stress–strain curves in samples Q&P and HSQ&P.

Conclusions

It was possible to confirm significant C enrichment of γ and depletion of C content in α', after the Q&P and HSQ&P processes. The HSQ&P samples showed the highest carbon enrichment in the austenitic phase when compared with the Q&P sample. The main reason for this higher carbon enrichment in HSQ&P samples could be the contribution of the formation of proeutectoid ferrite and α_{SITF}, and the C partitioning into γ from the supersaturated α', while the Q&P sample only receives a carbon contribution from the formation of proeutectoid α and the α' during the partition stage. In addition, high temperature deformation carried out before Q&P process can contribute to multiphase microstructure refinement, improving strength and ductility, owing to the occurrence of the TRIP effect associated with increased volumes of retained austenite. Although the partitioned specimens had their mechanical strength reduced, they achieve higher total elongation, increasing the absorbed energy and compensating performance.

Acknowledgments. The authors gratefully acknowledge financial support from CAPES – (Process nº 1715938). The Brazilian Synchrotron Light Laboratory (LNLS) and Brazilian Nanotechnology National Laboratory (LNNano) are also acknowledged for the use of the XTMS facility. APT measurements were conducted at ORNL's Center for Nanophase Materials Sciences (CNMS), which is a U.S. DOE Office of Science User Facility.

References

[1] Q. Han, Y. Kang, X. Zhao, N. Stanford, M. Cai, Mater. Des. 51 (2013) 409–414.
[2] I.Y. Pyshmintsev, M. Meyer, B.C. Cooman, R.A. Savray, V.P. Shveykin, M. Vermeulen, Metall. Mater. Trans. A 33A (2002) 1659–1667.
[3] J. Speer, D.K. Matlock, B.C. De Cooman, J.G. Schroth, Acta Mater. 51 (2003) 2611–2622.
[4] Y. Toji, G. Miyamoto, D. Raabe, Acta Mater. 86 (2015) 137–147.
[5] A.J. Clarke, J.G. Speer, M.K. Miller, R.E. Hackenberg, D.V. Edmonds, D.K. Matlock, F.C. Rizzo, K.D. Clarke, E. De Moor, Acta Mater. 56 (2008) 16–22.
[6] E.A. Ariza, J. Poplawsky, W. Guo, K. Unocic, A.J. Ramirez, A.P. Tschiptschin, S.S. Babu, Metall. Mater. Trans. A 49 (2018) 4809–4823.
[7] E.A. Ariza, M. Masoumi, A.P. Tschiptschin, Mater. Sci. Eng. A 713 (2018) 223–233.
[8] E.A. Ariza, A.S. Nishikawa, H. Goldenstein, A.P. Tschiptschin, Mater. Sci. Eng. A 671 (2016) 54–69.
[9] Y. Chang, G. Li, C. Wang, X. Li, H. Dong, J. Mater. Eng. Perform. 24 (2015) 3194–3200.
[10] C. Ghosh, V. V. Basabe, J.J. Jonas, Y.M. Kim, I.H. Jung, S. Yue, Acta Mater. 61 (2013) 2348–2362.